12th International Symposium on Turbulence and Shear Flow Phenomena (TSFP12)
Osaka, Japan (Online), July 19-22, 2022

POD AND DMD MODE ANALYSES OF POISEUILLE AND COUETTE FLOWS OVER 1/2-CONTRACTION-RATIO FORWARD-FACING STEP

Toru Yamada
Graduate School of Engineering
Nagoya Institute of Technology
Gokiso-cho, Showa-ku, Nagoya, Japan
email: yamada.toru@nitech.ac.jp

Takumi Sugisaka
Graduate School of Engineering
Nagoya Institute of Technology
Gokiso-cho, Showa-ku, Nagoya, Japan
email: yamada.toru@nitech.ac.jp

Shinji Tamano
Graduate School of Engineering
Nagoya Institute of Technology
Gokiso-cho, Showa-ku, Nagoya, Japan
email: tamano.shinji@nitech.ac.jp

Yohei Morinishi
Graduate School of Engineering
Nagoya Institute of Technology
Gokiso-cho, Showa-ku, Nagoya, Japan
email: morinishi.yohei@nitech.ac.jp

ABSTRACT

In this study, a set of experiments is conducted to investigate Poiseuille and Couette type turbulent channel flows over a forward-facing step (FFS) having a contraction ratio of 0.5. The Reynolds numbers are 3000 for both flows, which are based on channel height and channel center velocity in the downstream region. The flows are taken by a high speed camera and the instantaneous velocities are obtained by the PIV method. Proper orthogonal decomposition (POD) and dynamic mode decomposition (DMD) methods are applied to the instantaneous streamwise velocity fields. The results show that the dominant flow structures extracted by using those analyses are different to each other. The cause of this difference is considered to be due to the difference in the treatment of temporal information between the two methods. The DMD method was also applied to three different FFS flow types, and the analysis found three characteristic flow structures common to all the tested flow types.

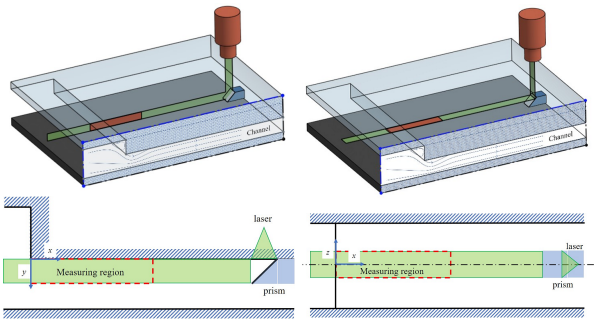

(a) (b)

Figure 1. Schematics of experimental setup (PIV measurement around the step downstream). (a) Three dimensional (upper) and side (lower) views for the vertical $(x-y)$ plane measurements. (b) Tree dimensional (upper) and top (lower) views for the horizontal $(x-z)$ plane measurements.

Introduction

Flow separation and reattachment are often encountered in the flows around vehicle body and in fluid machineries, and they cause negative impacts, such as increase in drag and pressure oscillation. Therefore, better understanding and controlling them are expected to enhance the energy efficiencies of those engineering applications. Turbulent flow over a forward-facing step, FFS, is a representative research object to study the characteristics of flow separation and reattachment. Tremendous researches on the separation and reattachment phenomena have been conducted to date. They are, however, mainly on flows over a backward-facing step, BFS, (cf., Chen *et al.* (2018)). These phenomena on a forward-facing step have also actively been investigated (Fang *et al.* (2021)) but still relatively less studied when compared to the study on BFS flows.

One blind spot in the studies of FFS flows is effects of flow types on the separation and reattachment. The FFS flows have been studied for boundary-layer type flow and channel type flow conditions. In the present study, the channel type flow is focused because it is simpler as boundary layer thickness does not have to be taken into account. The channel type flows can be further categorized as Poiseuille (P) type, Couette at step upstream (C_{su}) type, and Couette at step downstream (C_{sd}) type flows. It expected that the separation and reattachment phenomena can be influenced by these flow types. However, it is extremely difficult to find a study focusing on the effect of these flow types in the existing works.

Another interesting topic of interest is extraction of characteristic flow structures associated with the separation and reattachment phenomena. Previous studies have found that the separation regions attached on a FFS temporally change their size and shape (Stüer *et al.* (1999); Sherry *et al.* (2010)). Its three dimensional characteristics has also been focused on in a recent study (Fang *et al.* (2021)). Our research group also implemented both the PIV and the DNS studies for the Couette type FFS flows focusing on counter gradient diffusion phenomenon of the Reynolds stress in the vicinity of the separation bubble at the FFS downstream (Morinishi *et al.* (2017)). The spatial and temporal characteristics of these flow structures can be effectively extracted by modal decomposi-

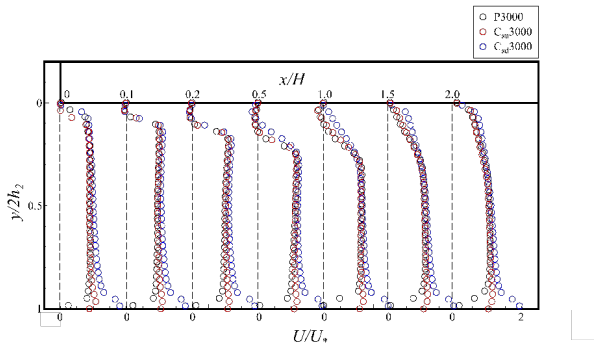

Figure 2. Mean velocity profiles at different x locations for $x/2h_2 \leq 2.0$ (U_* is either U_{c_2} or $\frac{1}{2}U_w$ for the P3000 and $C_{su}3000$ flows or the $C_{sd}3000$ flow).

tion methods, and the proper orthogonal decomposition (POD) method has been used for the FFS flow studies (Yang *et al.* (2019)). In POD analyses, temporal information was rarely extracted due to the use of insufficiently time-resolved data. Therefore, the discussions about temporal characteristics of flow structures have not been adequately made in FFS flow studies.

Present study experimentally investigates the effect of the different channel type flows on the FFS flow characteristics. Two mode decomposition methods are used to analyse the experimental data, i.e. the POD method and the dynamic mode decomposition (DMD) method which are both widely well-known coherent structure analyses in fluid dynamics (Kutz *et al.* (2016)). The differences in flow behaviors among the tested flow types are evaluated through the POD and DMD analyses, and meanwhile, the difference in flow characteristics extracted from the mode analyses is also discussed.

EXPERIMENTAL METHODOLOGY

Experimental setup

Figure 1 shows the schematics of the experimental setup to obtain the data for the mode analyses in the present study where the left (Fig. 1(a)) and right (Fig. 1(b)) of the figure are the diagrams of the vertical ($x-y$) and horizontal ($x-z$) plane measurements, respectively. Note that, as shown in Fig. 1(a), the sheeted laser is exposed in the upper half region for the $x-y$ plane measurement which leads to the POD and DMD analyses of the velocity fields available only in the region. The air involving olive oil mist flows into the test section (parallel-plate channel with 865 mm in width). The flow experiences a sudden contraction at the FFS located at the distance of 3500 mm downstream of the channel inlet and finally exits from the channel outlet. Either Couette flow or Poiseuille flow can be created by activating or deactivating the lower moving wall.

In this study, the contraction ratio, CR (= h_2/h_1 where h_1 and h_2 are the half heights of the channel upstream and downstream the FFS, respectively) is set to be constant at 0.5, and the Reynolds number is kept at 3000 regardless of flow types. Thus the results for the Poiseuille and the two Couette flows are called as P3000, $C_{su}3000$, and $C_{sd}3000$, respectively. The Reynolds number for the Poiseuille flow is defined as $Re = U_{c_2}(2h_2)/\nu$, where U_{c_2} is the channel-center velocity for the fully-developed downstream flow and ν is kinematic viscosity of air. The Reynolds numbers for the C_{su} and C_{sd} flows are respectively defined as $Re = \frac{1}{2}U_w(2h_1)/\nu$ and $Re = \frac{1}{2}U_w(2h_2)/\nu$, where U_w is the velocity of the moving wall. The flows are taken by a high speed camera with a frame rate of 6000 Hz and the instantaneous velocity fields are obtained by the PIV method. The POD and DMD methods are applied to the streamwise velocity and the difference of flow characteristics among the three flow types is discussed.

Proper orthogonal decomposition (POD)

The POD method is a way of decomposing a data matrix by using the singular value decomposition (SVD). It is a very useful method to extract a hierarchical set of orthogonal modes from a dynamics system (Kutz *et al.* (2016)). When the POD method is applied to analyze velocity fields, the snapshots of velocity data of flow field are synthesized into a matrix $\mathbf{X}$, i.e., $\mathbf{X} = [\mathbf{x}_1, \mathbf{x}_2, \cdots, \mathbf{x}_k]$ where $\mathbf{x}_k$ is the snapshot of velocity data. In the POD method the matrix does not have to be synthesized in chronological order in case that temporal information is not required. The SVD of $\mathbf{X}$ is taken such that $\mathbf{X} = \mathbf{U}\Sigma\mathbf{V}^*$ where the star indicates the conjugated transpose. In the POD method, the space and time correlations are obtained from the matrices $\mathbf{U}$ and $\mathbf{V}$, respectively. The matrix $\mathbf{U}$ contains the spatial information, i.e. the POD modes, and is obtained by $\mathbf{U} = \mathbf{X}\mathbf{V}\Sigma^{-1}$after computing Σ and $\mathbf{V}$ from spectral decomposition of $\mathbf{X}^*\mathbf{X}$ (Kutz *et al.* (2016)). $\mathbf{V}$ contains the time information of the corresponding POD modes. It is in the form of spectra including multiple characteristic frequency of the modes. This is one of the fundamental differences between the POD and DMD methods where each DMD mode has only one frequency. This time related information would be meaningless when using non-time-resolved data.

Dynamic mode decomposition (DMD)

The DMD method spatio-temporally decomposes experimental or numerical data into a set of dynamic modes. Although the DMD method also utilizes a similar matrix to $\mathbf{X}$, the snapshot $\mathbf{x}_k$ must be synthesized in chronological order in the DMD method. It is assumed in the DMD method that the linear relationship, $\mathbf{X}_1 = \mathbf{A}\mathbf{X}_0$, holds, where $\mathbf{X}_0 = [\mathbf{x}_1, \mathbf{x}_2, \cdots, \mathbf{x}_{k-1}]$ and $\mathbf{X}_1 = [\mathbf{x}_2, \mathbf{x}_3, \cdots, \mathbf{x}_k]$. This means that the time marching of vector $\mathbf{x}$ is expressed by the linear mapping via the $\mathbf{A}$ matrix. The $\mathbf{A}$ matrix is obtained such that Frobenius norm $\|\mathbf{X}_1 - \mathbf{A}\mathbf{X}_0\|_2^2$ is minimized. In the DMD method, the eigenvectors of $\mathbf{A}$, ϕ, and corresponding eigenvalues, μ, are obtained in a similar way to the POD method, i.e., the SVD is used. The eigenvectors are called the DMD modes. A simple solution to the above relationship can be expressed as $\mathbf{x}_{k+1} = \sum_j^r \phi_j \mu_j b_j$ where b is the coefficients of initial condition, the subscript j indicates DMD mode number, and r is the total number of DMD modes. Thus, it is important to compute the eigenvectors and eigenvalues with a time effective algorithm.

A specific procedure to obtain ϕ and μ is briefly expressed as follows. The size of $\mathbf{A}$ is usually unrealistically large to be directly solved. Therefore, the SVD of the matrix $\mathbf{X_0} = \mathbf{U}\Sigma\mathbf{V}^*$ is substituted into the above relationship so as to obtain a matrix $\tilde{\mathbf{A}} = \mathbf{U}^*\mathbf{X}_1\mathbf{V}\Sigma = \mathbf{U}^*\mathbf{A}\mathbf{U}$ which takes over the information of $\mathbf{A}$ in a contracted form. The relationship of eigenvectors and eigenvalues between $\mathbf{A}$ and $\tilde{\mathbf{A}}$ is $\phi_j = X_0 V \Sigma^{-1}\phi_{\tilde{\mathbf{A}}_j}$ and $\mu_j = \mu_{\tilde{\mathbf{A}}_j}$. This algorithm is called exact DMD and is used in this study.

RESULTS AND DISCUSSION

The flow separation and reattachment of flow over a FFS are often characterized by the quasi-periodic dynamics (in the

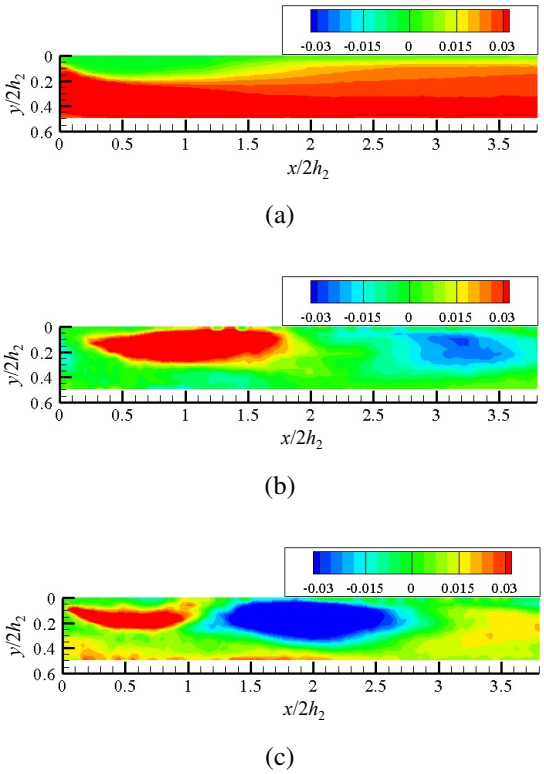

Figure 3. POD modes of ϕ_u for the $x-y$ plane, P3000: (a) Mode 1, (b) Mode 2, and (c) Mode 3.

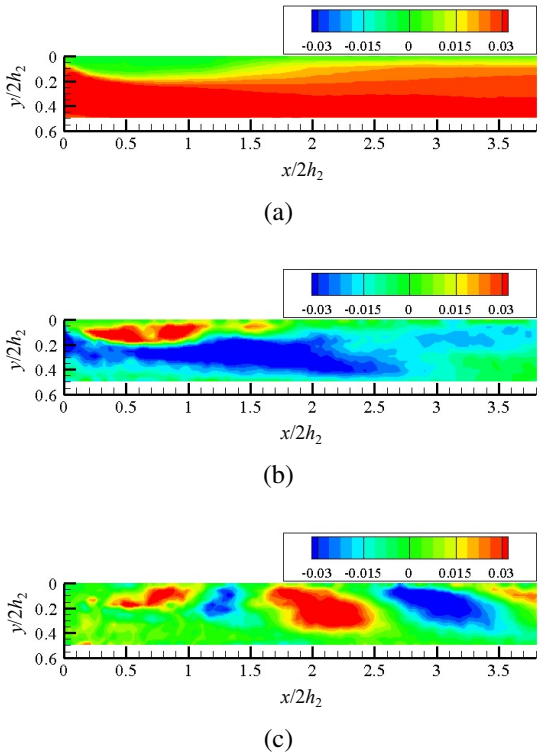

Figure 4. DMD modes of ϕ_u for the $x-y$ plane, P3000: (a) Mode 1, (b) Mode 4, and (c) Mode 8.

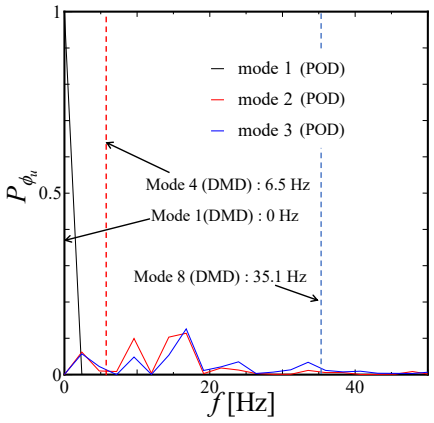

Figure 5. Power spectra of the POD modes shown in Fig. 3 where the mode frequencies of the DMD modes shown in Fig. 4 are simultaneously presented with vertical lines.

spanwise direction) of separation bubbles generated on the step. The bubble generated in the downstream of the step repeats its enlargement and contraction with evolving vortices during the dynamics. Characteristic flow structures of dynamics of the separation bubble can be coherently extracted by the POD and DMD analyses.

Mean flow profiles

Figure 2 shows the mean velocity profiles for the flows of P3000, $C_{su}3000$ and $C_{sd}3000$ at different locations along the downstream of the channel. It should be mentioned that these results were obtained by using a system with a double-puls laser and a CCD camera which is different from the one used for the POD and DMD analyses. There are regions near the upper (stationary) wall in which the velocity is negative. This is an indication of the existence of the flow separation. For P3000 and $C_{su}3000$ flows, the regions are extended to around $x/2h_2 = 1.5$. For the $C_{sd}3000$ flow, it appears to be relatively small because the negative-velocity region can be observed up to $x/2h_2 = 1.0$. The velocity profiles near the lower (lower) wall for the three flow types are different to each other. For the P3000 flow, the velocity approaches to zero because the lower wall is kept stationary. The velocity for the Couette flows, on the other hand, approaches to non-zero moving wall velocity. The difference between the $C_{su}3000$ and $C_{sd}3000$ flows is that the velocity above the moving wall becomes greater than the wall velocity for the C_{su} flow. The reason is considered that the virtual flow-passage area has shrunk due to the separation region at the upper wall for this flow condition.

Comparison between the POD and DMD modes

In this subsection, the characteristic differences between the POD and DMD analyses are discussed by means of the streamwise velocity data on the $x-y$ plane for the P3000 flow. Figure 3 shows the first three modes of the instantaneous streamwise velocity field for P3000 obtained by the POD analysis. Also, Fig. 4 shows the characteristic three modes obtained by the DMD analysis where these modes selected by machine learning with the greedy algorithm proposed by Ohmichi (2017). Note that, for the DMD modes, either complex conjugated modes or very similar modes to the indicated ones are omitted for simplicity. The comparison between Figs. 3 and 4 shows that the first mode for both analyses is almost identical. This mode appears to represent the mean velocity field because the characteristic is closely similar to that of the field, including separation region at the corner of the step and flow covering the separation. However, the other

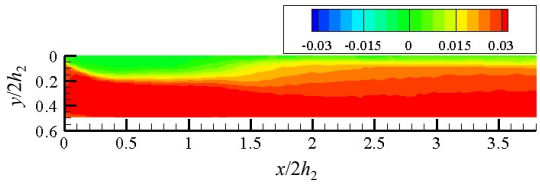

(a)

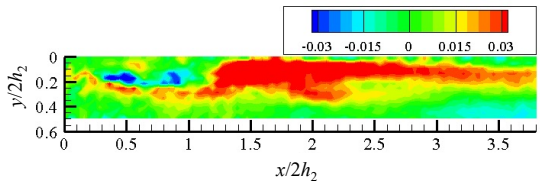

(b)

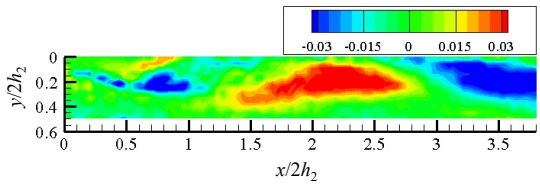

(c)

Figure 6. DMD modes of ϕ_u for the x-y plane, $C_{su}3000$: (a) Mode 1 ($f = 0$ Hz), (b) Mode 7 ($f = 18.5$ Hz) , and (c) Mode 24 ($f = 30.1$ Hz).

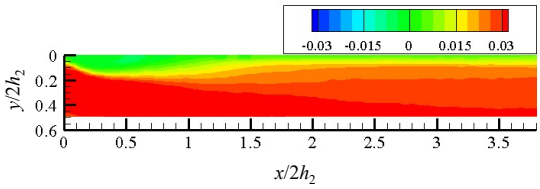

(a)

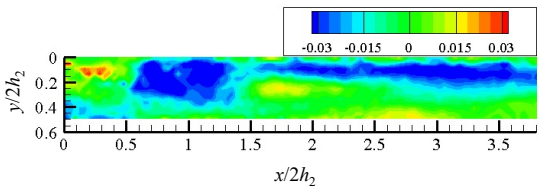

(b)

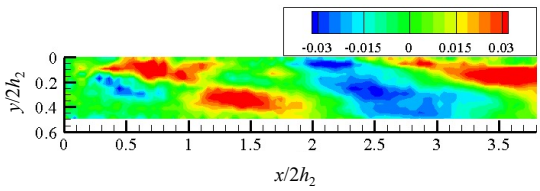

(c)

Figure 7. DMD modes of ϕ_u for the x-y plane, $C_{sd}3000$: (a) Mode 1 ($f = 0$ Hz), (b) Mode 8 ($f = 12.1$ Hz), and (c) Mode 16 ($f = 26.8$ Hz).

modes obtained by the POD and DMD analyses do not correspond well to each other. The contour plots of these modes in both POD and DMD analyses are reminiscent of longitudinal vortex stretched to the channel downstream (DMD mode 4) and vortex shedding from the separation bubbles (POD modes 2 and 3, and DMD mode 8) which can be observed via instantaneous flow fields. The analytical results must be compared with other quantitative data such as turbulence statistics to further investigate the flow structures extracted by these analyses, which is one of our future works.

This difference in dominant modes extracted between the POD and DMD analyses is considered to be due to the difference in expression of teomporal information: The POD method allows a POD mode to have multiple frequency whereas the DMD method limits one DMD mode to occupying one frequency. In the POD analysis, similar flow structures may be integrated together as one POD mode, which may lead to obscuring their temporal characteristics. This could one main reason for the POD method being unsuitable for complex three-dimensional flows, e.g. the present FFS flows, as reported by Higham *et al.* (2018).

Figure 5 shows the frequency characteristics of the POD and DMD modes presented in Figs. 3 and 4. As can be seen in this figure, the frequencies of the first mode for both analyses are zero, which is considered to prove that this mode represents the mean velocity field. The other dominant frequencies of the POD modes, however, only moderately correspond well to those of the DMD modes. This difference is considered to be due to the POD characteristics mentioned earlier, i.e. the potential of obscuring the peaks by integrating spatially similar flow structures. In the DMD analysis, on the other hand, the flow structures are decomposed completely in terms of frequency regardless of their spatial similarity. This difference is considered to have led to the mismatch between the POD and DMD analyses. The comparison between the POD and DMD analyses shows that the DMD method has more ability to capture the feature of time evolution of flow structures than the POD method. Whereas, the superiority of the POD method is that it requires fewer number of mode to reconstruct flows due to no frequency limitation included in each mode. Therefore, it can be said that the choice of modal decomposition method is derived by importance of the time evolution of flow structures and time resolution of the data.

DMD modes of the x-y plane

This and subsequent sections show the comparisons of the DMD modes for streamwise velocity fields on the $x-y$ and $x-z$ planes, respectively, among the P3000, $C_{su}3000$, and $C_{sd}3000$ flows, and the difference in spatio-temporal structures is discussed.

Figure 6 show the characteristic DMD modes for the $x-y$ plane for the $C_{su}3000$ flow where f denotes the frequency of each DMD mode and is the same for subsequent figures. The same algorithm (Ohmichi (2017)) has been used for the mode selection. As can be seen in Fig. 6(a), Mode 1 seems to be the mean flow field which is the same as the P3000 flow. This indicates that the mean flow is the flow structure making a contribution regardless of flow types. Next, Mode 7 in Fig. 6(b) looks very similar to Mode 4 in Fig. 4(b). However, the frequency of the former is 18.5 Hz which is greater than that for the latter. Actually, there are several spatially similar structures extracted in lower ranked DMD modes which have a range of frequencies less than 20 Hz. Thus, there might be a DMD mode having a similar frequency as Mode 4 of P3000 flow while it was ranked as less-dominated DMD mode by the greedy algorithm. This is considered to the reason of the difference in frequency between Fig. 6(b) and Fig. 4(b) instead

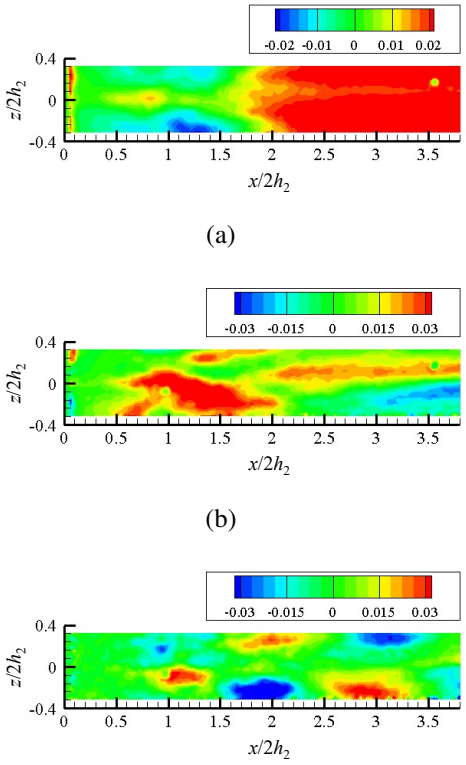

Figure 8. DMD modes of ϕ_u for the $x-z$ plane, P3000: (a) Mode 1 ($f = 0$ Hz), (b) Mode 3 ($f = 4.3$ Hz), and (c) Mode 9 ($f = 30.6$ Hz).

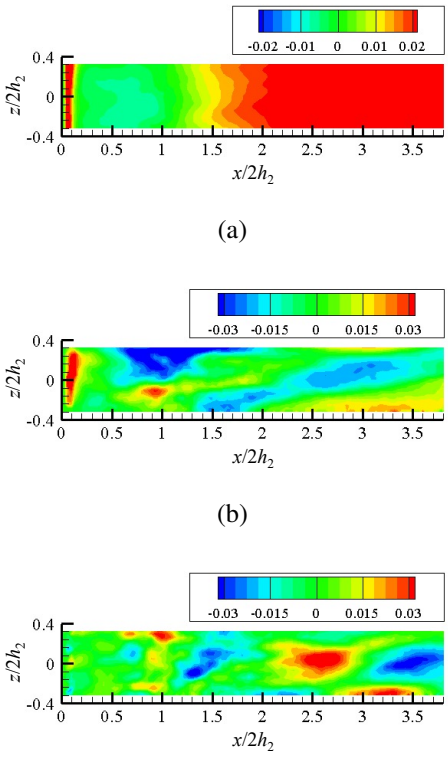

Figure 9. DMD modes of ϕ_u for the $x-z$ plane, $C_{su}3000$: (a) Mode 1 ($f = 0$ Hz), (b) Mode 6 ($f = 15.2$ Hz), and (c) Mode 20 ($f = 32.5$ Hz).

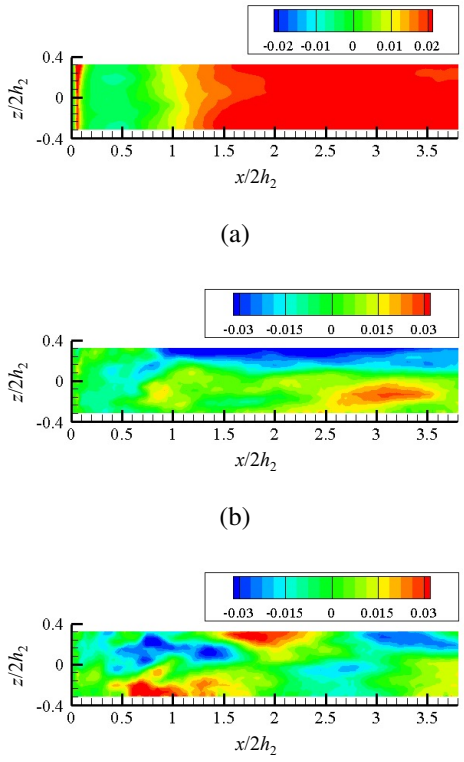

Figure 10. DMD modes of ϕ_u for the $x-z$ plane, $C_{sd}3000$: (a) Mode 1 ($f = 0$ Hz), (b) Mode 4 ($f = 6.1$ Hz), and (c) Mode 16 ($f = 27.4$ Hz).

of their flow types. Mode 24 in Fig. 6(c) seems to show the vortex shedding from the separation bubble. This mode looks similar to Fig. 4(c). The size of the shedded vortex is larger than that shown in P3000 flow while the frequency is almost the same. However, the ranking of this mode (Mode 24) is much lower than that for P3000 (Mode 8), indicating that the importance of vortex shedding may differ according to flow types.

Figure 7 shows the characteristic modes for the $x-y$ plane for the $C_{sd}3000$ flow. As can be seen in Fig. 7(a) and (b), these modes seem to extract the mean velocity flow field and longitudinal vortex stretched to the channel downstream. These two modes are very similar to the foregoing DMD modes for the P3000 and $C_{su}3000$ flows while the separation bubble is slightly smaller. A noticeable difference in the flow structure to the other flow types can be seen in Fig. 7(c). This mode (Mode 16) seems to indicate the vortex shedding from the separation bubble which is the same to the other types. However, the shape of the vortices is different. The shedded vortex for $C_{sd}3000$ looks triangular shape where it is expanded in both the x and y directions. Whereas, the vortices for the other flow types look more elliptic shape meaning that the vortex stretched only in the x direction. The cause of this difference remains unclear yet and some modification of experimental setup might be necessary to capture the flow across the entire y-direction, i.e. $0 < y/H < 1$.

DMD modes of the x-z plane

Figure 8 shows the characteristic DMD modes for the $x-z$ plane for the P3000 flow. Firstly, Fig. 8(a) should be the mean velocity field as this mode is stationary (zero frequency).

The reattachment point of the separation bubble is inferred at $1.5 < x/H < 2.0$ in which the contour color is changing from green to red. This region corresponds to the one expressed in our earlier consideration about Fig. 2. Secondly, it can be seen from Fig. 8(b) that a longitudinal vortex is stretched to the channel downstream from the reattachment point. The frequency of this mode is 4.3 Hz. The structure and temporal characteristics are correspondent well to Mode 2 for the $x-y$ plane (Fig. 4(b)). Similarly, the characteristics of Mode 9 in Fig. 8(c) is in accordance well with Mode 8 for the $x-y$ plane where the frequency for the Mode 9 is 30.6 Hz. Therefore, it can be said that the dominant modes of the streamwise velocity for the $x-y$ and $x-z$ planes extracted by the DMD method are almost identical to each other.

Figure 9 shows some of dominant DMD modes for the $x-z$ plane for the $C_{su}3000$ flow. What is observed from this figure is very similar to that from the P3000 flow (Fig. 8). One of distinctions of the $C_{su}3000$ flow is that the longitudinally stretched vortex shown in Mode 6 (Fig. 9(b)) is slightly inclining to the spanwise (z) direction as compared to Mode 3 for the P3000 flow (Fig. 8(b)). Also, the structure of the vortex shedding (Mode 20 in Fig. 9(c)) is a relatively higher mode compared to the similar structure for the P3000 flow (Mode 9 in Fig. 8(c)). This indicates that the vortex shedding is not dominant for the $C_{su}3000$ flow. Overall, it is observed from the results that the structure and temporal characteristics of the DMD modes for the $x-z$ plane correspond well with those for the $x-y$ plane for the $C_{su}3000$ flow.

Figure 10 shows some of dominant DMD modes for the $x-z$ plane for the $C_{sd}3000$ flow. Fig. 10(a) appears to be the mean velocity field similarly to the results for the other flow types. Whereas, the change in contour color occurs around $x/H > 1$, indicating that the size of separation bubble is smaller for the $C_{sd}3000$ flow. Also, it can be seen from Fig. 10(b) that the longitudinally stretched vortex arises the region closer to the FFS compared to the other flow types. In addition, characteristic structure of vortex shedding is not observed for the $x-z$ plane unlike the results of the $x-y$ plane (Fig. 7(c)). This expresses that the difference in spatial structure and temporal behavior of the $C_{sd}3000$ flow is more prominent in the $x-y$ plane.

The summary of the DMD analyses for the three different flow types is as follows. The DMD modes can be categorized into three classifications in terms of their spatial structure and temporal frequency. First part is the mean velocity field with zero frequency which is considered to be the most dominant structure for all the flow types. Second part is the structure of longitudinally-stretched vortex having relatively small frequencies ranging from single- up to double-digits values, which is the second most dominant structure. Third part is the structure of vortex shedding of which the degree of contribution to entire flow dynamics depends on flow types.

CONCLUSION

Poiseuille and Couette type turbulent channel flows over a forward-facing step, having a contraction ratio of 0.5, were experimentally investigated in the present study. These experimental data was analyzed via the POD and DMD methods, and the modes extracted between these methods were compared. Also, the DMD modes extracted from the streamwise velocity fields for different flow types, P3000, $C_{su}3000$, and $C_{sd}3000$, were compared. The main findings from the present study are listed as follows. First, it was found from the comparison between the POD and DMD analyses, the first modes extracted by both analyses corresponded to each other, and the modes were considered to represent the mean flow structure because the frequency was calculated to be null in both analyses. Second, the other modes extracted were different between the POD and DMD analyses. The discrepancy was considered to be due to the difference in expression of temporal information between the POD and DMD methods. The DMD mode analyses for the three flow types found that the flow structures can be characterized into the following three parts in terms of their spatial structure and temporal frequency. First part is the mean velocity field with zero frequency which is considered to be the most dominant structure for all the flow types. Second part is the structure of longitudinally-stretched vortex having relatively small frequencies ranging from single- up to double-digits values, which is the second most dominant structure. Third part is the structure of vortex shedding of which the degree of contribution to entire flow dynamics depends on flow types.

ACKNOWLEDGEMENTS

This study is financially supported by JSPS-KAKENHI Grant-number JP20H02064. Also, the figures were partly generated by Mr. Koki Izumika, a graduate student at Nagoya Institute of Technology.

REFERENCES

Chen, L., Asai, K., Nonomura, T., Xi, G. & Liu, T. 2018 A review of backward-facing step (bfs) flow mechanisms, heat transfer and control. *Thermal Science and Engineering Progress* **6**, 194–216.

Fang, X., Tachie, M. F., Bergstrom, D. J., Yang, Z. & Wang, B. 2021 Three-dimensional structural characteristics of flow separation induced by a forward-facing step in a turbulent channel flow. *Journal of Fluid Mechanics* **919**, A24.

Higham, J. E., Brevis, W. & Keylock, C. J. 2018 Implications of the selection of a particular modal decomposition technique for the analysis of shallow flows. *Journal of Hydraulic Research* **56** (6), 796–805.

Kutz, J. N., Brunton, S. L., Brunton, B. W. & Proctor, J. L. 2016 *Dynamic mode decomposition: data-driven modeling of complex systems*. SIAM.

Morinishi, Y., Kubota, S., Tamano, S. & Yamada, T. 2017 Turbulence structure leading to unsteady upstream separation in Couette flow with forward-facing step. In *Proc. of Tenth International Symposium on Turbulence and Shear Flow Phenomena*, Chicago, USA, 2C5, 1–6.

Ohmichi, Y. 2017 Preconditioned dynamic mode decomposition and mode selection algorithms for large datasets using incremental proper orthogonal decomposition. *AIP Advances* **7** (7), 075318.

Sherry, M., Jacono, D. L. & Sheridan, J. 2010 An experimental investigation of the recirculation zone formed downstream of a forward facing step. *Journal of Wind Engineering and Industrial Aerodynamics* **98** (12), 888–894.

Stüer, H., Gyr, A. & Kinzelbach, W. 1999 Laminar separation on a forward facing step. *European Journal of Mechanics-B/Fluids* **18** (4), 675–692.

Yang, S. Q., Wang, Y., Yang, M., Song, Y. & Wu, Y. 2019 Pod-based data mining of turbulent flows in front of and on top of smooth and roughness-resolved forward-facing steps. *IEEE ACCESS* **7**, 18234–18255.